

# Modeling of thermal contacts with heat generation: Application to electrothermal problems

Anas El Maakoul, Benjamin Remy, Alain Degiovanni

► **To cite this version:**

Anas El Maakoul, Benjamin Remy, Alain Degiovanni. Modeling of thermal contacts with heat generation: Application to electrothermal problems. *International Journal of Heat and Mass Transfer*, Elsevier, 2019, 140, pp.293-302. 10.1016/j.ijheatmasstransfer.2019.06.015 . hal-02441295

**HAL Id: hal-02441295**

**<https://hal.univ-lorraine.fr/hal-02441295>**

Submitted on 25 Oct 2021

**HAL** is a multi-disciplinary open access archive for the deposit and dissemination of scientific research documents, whether they are published or not. The documents may come from teaching and research institutions in France or abroad, or from public or private research centers. L'archive ouverte pluridisciplinaire **HAL**, est destinée au dépôt et à la diffusion de documents scientifiques de niveau recherche, publiés ou non, émanant des établissements d'enseignement et de recherche français ou étrangers, des laboratoires publics ou privés.



# 1            **Modeling of thermal contacts with heat generation: application to electrothermal problems**

2    Anas El Maakoul <sup>b\*</sup>, Benjamin Remy <sup>a</sup>, Alain Degiovanni <sup>a,b</sup>

3    <sup>a</sup> Université de Lorraine, CNRS, LEMTA, 54504 cedex, Vandoeuvre les Nancy, France

4    <sup>b</sup> Université Internationale de Rabat, Pôle Energie, LERMA, 11100 Sala Al Jadida, Maroc

5    Abstract:

6    When modeling thermal contacts with heat generation between two solids (e.g. electrothermal  
7    applications), we are often interested in evaluating the heat transfer rates and contact temperatures,  
8    and generally, it is difficult to evaluate these thermal characteristics due to interfacial conditions. In  
9    this work, a general representation of solid-solid thermal contact problems with heat generation is  
10    proposed. This representation is based on the thermal-electrical analogy and uses the notion of  
11    partition coefficient  $\beta$ . The resulting equivalent thermal circuits are presented and discussed. The  
12    pertinence of this analytical approach is demonstrated for the electrothermal application of Joule  
13    heating for different contact configurations (similar and dissimilar materials, with and without  
14    interstitial fluid). The analytical results for each configuration are compared to numerical results  
15    obtained using numerical simulations under similar conditions, both results are in very good  
16    agreement.

## 17    **1. Introduction:**

18    Modeling thermal contacts problems with heat generation is both complex and difficult. This difficulty  
19    comes mainly from modeling the interfacial conditions, and until now, to the authors knowledge, there  
20    is no model or method that received unanimous acceptance by the heat transfer community.

21    In the literature, there are numerous studies where different models are proposed and applied to  
22    various applications of thermal contacts with heat generation. Depending on the application, two  
23    mains categories can be identified: Contacts with friction (molding, machining, ...) and electrothermal  
24    contacts (electrical conductors, spot welding process ...).

25    A description of representative studies that appear in the literature now follows. For the first category  
26    of contacts with friction, several research works dealt with machining and molding [1-4], while in  
27    others, the authors studied dry contact under perfect contact conditions [5-10] or Imperfect contact  
28    conditions [11-14]. The heat generated through friction was evaluated differently depending on the  
29    authors. Some distributed the heat sources [15,16], some located the heat generation on the contact  
30    plane [17], others located it on one of the friction surfaces [18]. Other authors, based on the approach  
31    used by Bardon [19], considered interfacial heat generation using the notion of ‘part of the generated  
32    heat that causes a spike in temperature at the interface’ or ‘heat generation factor’ [20-24]. As for the  
33    second category of electrothermal contacts, heat is generated in the matter of the materials in contact.  
34    There are various models for this category, such as with or without contact resistance and with or  
35    without interfacial heat generation [25-33].

36    The foregoing short introduction shows that the main difficulty lies in the representation of the heat  
37    sources, particularly if we want to keep the notion of “contact resistance”. One representation that  
38    can be generalized was introduced by Bardon [19] which, as mentioned previously, consists in  
39    considering interfacial heat generation and introducing a heat generation factor  $\alpha$ , the equivalent  
40    thermal circuit for this representation is shown in figure 1. In this case,  $R_1$  and  $R_2$  are respectively the  
41    non-perturbed thermal resistances of mediums 1 and 2,  $R_c$  is the contact resistance and  $\varphi_g$  the total  
42    rate of heat generation.

43 In this representation, the coefficient  $\alpha$  depends not only on the spatial distribution of the heat sources  
 44 but also on the thermal conductivities  $\lambda_1$  and  $\lambda_2$  of the mediums 1 and 2. Another problem with this  
 45 representation is that does not permit the evaluation of the contact temperature.

46 In this paper, we consider the solid-solid thermal contact problem with heat generation and propose  
 47 a general representation, that is easily applicable, to evaluate the heat transfer rates and contact  
 48 temperature. To do so, we first need to examine in detail the notion of “contact resistance”.

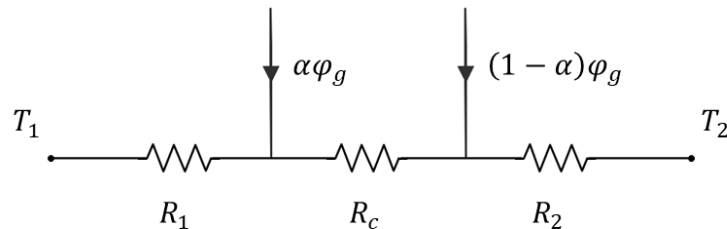


Figure 1: Equivalent thermal circuit proposed by Bardon [19]

49 **2. Concept of “contact resistance”:**

50 Let’s consider the contact between two solids without heat sources (figure 2), because the solid  
 51 contact spots are interspersed with gaps (that are generally filled with a fluid), the actual contact area  
 52 (solid contact spots) is much smaller than the apparent area. The contact resistance is described using  
 53 an axisymmetric elementary contact cell that corresponds to a reference contact area associated to a  
 54 rate of heat transfer; the overall contact and heat transfer are represented by multiple elementary  
 55 cells in parallel [34, 35] as shown in figure 2. Figure 3 represents schematically an elementary cell.

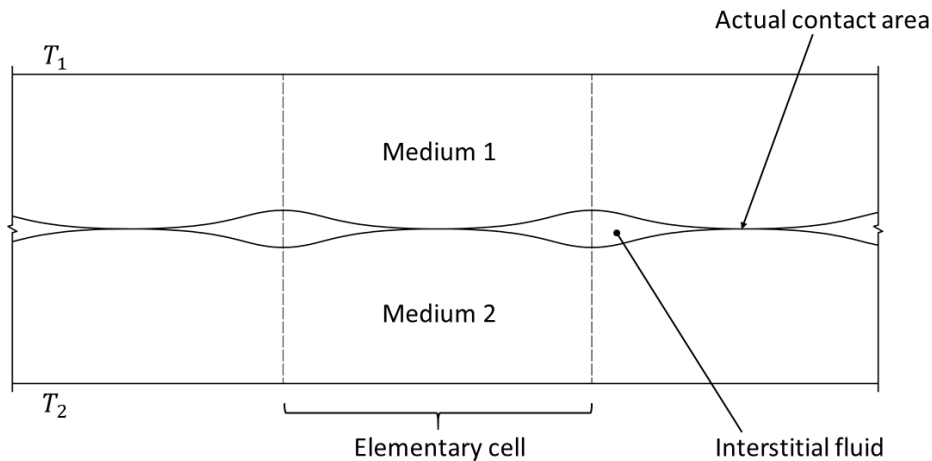


Figure 2: Representation of contact between two solids

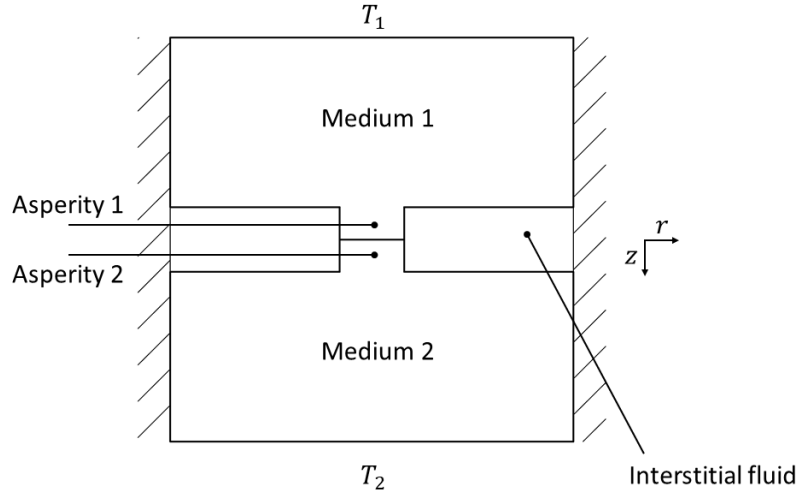


Figure 3: schematic representation of an axisymmetric elementary contact cell

56

57 With reference to figure 3, the rigorous approach consists in splitting the elementary cell into two  
 58 parallel heat transfer regions (internal and external). In the internal region, heat flows through the  
 59 asperities while in the external region heat flows through the interstitial fluid. The foregoing is  
 60 presented in figure 4.a, where the two regions are separated with dashed curves.

61 Noting that the total heat transfer is the sum of the heat transfer rates  $\phi_i$  and  $\phi_e$ , we can write:

$$\frac{1}{R_t} = \frac{1}{R_i} + \frac{1}{R_e} \quad (1)$$

62 Where  $R_t$  is the total thermal resistance,  $R_i$  and  $R_e$  are respectively the thermal resistances of the  
 63 internal and external regions. Let's decompose the resistance of each region into resistances  
 64 connected in series (figure 4.b and figure 5):

$$R_i = R_{m1i} + R_{c1i} + R_{a1} + R_{a2} + R_{c2i} + R_{m2i} \quad (2)$$

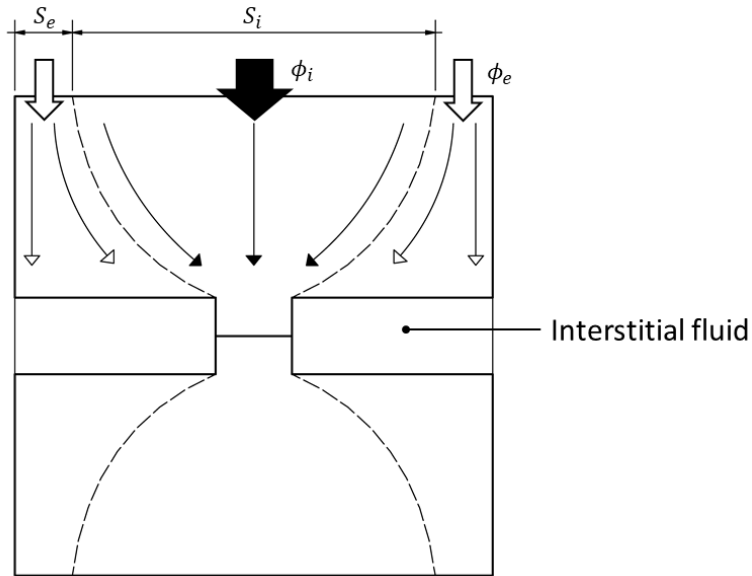
$$R_e = R_{m1e} + R_{c1e} + R_f + R_{c2e} + R_{m2e} \quad (3)$$

65 Where

- 66 •  $R_{m1i}$  and  $R_{m2i}$  represent the resistances associated to the surface  $S_i$  (internal region).
- 67 •  $R_{m1e}$  and  $R_{m2e}$  represent the resistances associated to the surface  $S_e$  (external region).
- 68 •  $R_{a1}$  and  $R_{a2}$  are the resistance of the asperities.
- 69 •  $R_f$  is the resistance of the fluid
- 70 •  $R_{c1i}$  and  $R_{c2i}$  are the constriction resistances associated to the internal region (narrowing heat  
 71 flow area, see figure 4)
- 72 •  $R_{c1e}$  and  $R_{c2e}$  are the constriction resistances associated to the external region (widening heat  
 73 flow area)

74

a)



b)

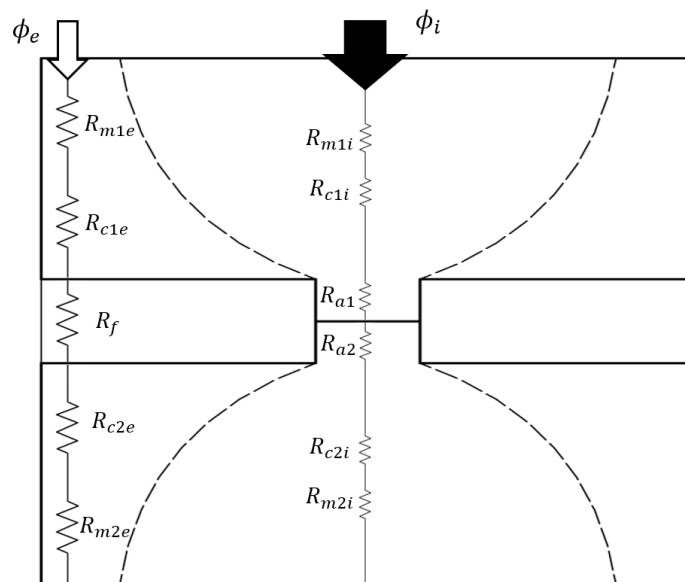


Figure 4: a) internal ( $\phi_i$ ) and external ( $\phi_e$ ) heat transfer regions for an elementary cell; b) thermal resistances in series for each region (Eq (2-3))

75

76 In figure 5, it can be demonstrated (see appendix 1) that the potentials  $A$  and  $C$  are the identical, the  
 77 same is true for the potentials  $B$  and  $D$ . Moreover, in most cases, the actual contact area is much  
 78 smaller than the apparent area, therefore the external constriction resistances ( $R_{c1e}$  and  $R_{c2e}$ ) are  
 79 negligible compared to the fluid resistance  $R_f$  and the internal constriction resistances are very close  
 80 to the intrinsic constriction resistances (irrespective of the asperities and the fluid) [36]. The inferred  
 81 thermal circuit is shown in figure 6 where  $R_c$  is the contact resistance.

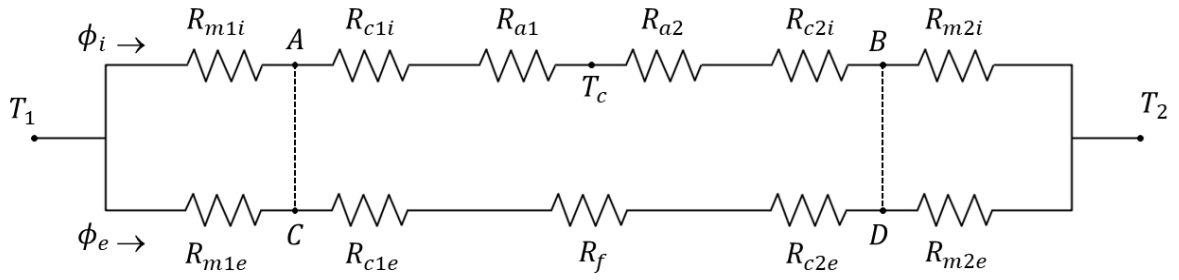


Figure 5: The complete equivalent thermal circuit for contact problems without heat source

82

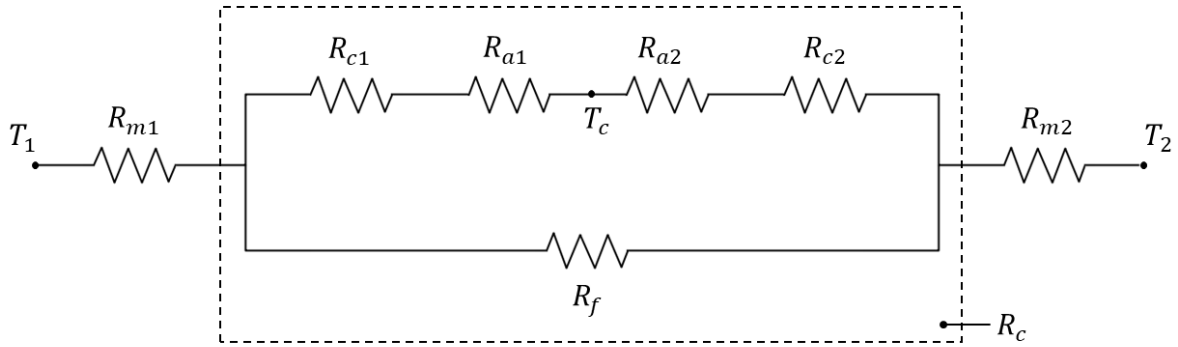


Figure 6: Simplified equivalent thermal circuit for contact problems without heat source

83

84 Can the preceding equivalent thermal circuit be modified to consider internal heat sources? in the case  
 85 of localized sources, the problem is solved by simply applying Kirchhoff's current law, while for a  
 86 distributed source (heat generation varying with position), it was demonstrated that the problem has  
 87 an equivalent thermal circuit [37]. In the next section, we briefly present this demonstration for the  
 88 special case of curvilinear coordinates.

### 89 3. Notion of partition coefficient in a steady conduction problem with an internal source [37]:

90 Let's consider the case of unidirectional conduction with internal sources where the heat flux vector is  
 91 perpendicular to the isothermal surfaces. The sources are uniform between two isotherms and we can  
 92 define a curvilinear coordinate  $s$  orthogonal to the isotherms (figure 7).

93 With  $g(s)$  the volumetric heat generation rate,  $S(s)$  the isothermal section and constant thermo-  
 94 physical properties, we can write Fourier's equation as:

$$\phi(s) = -\lambda S(s) \frac{dT(s)}{ds} \quad (4)$$

95 And the energy balance:

$$d\phi = g(s)S(s)ds \quad (5)$$

96 We define:

$$Q = \int_{s_{in}}^{s_{out}} g(s)S(s)ds \quad r(s) = \int_{s_{in}}^s \frac{ds}{\lambda S(s)} \quad R = \int_{s_{in}}^{s_{out}} \frac{ds}{\lambda S(s)}$$

97

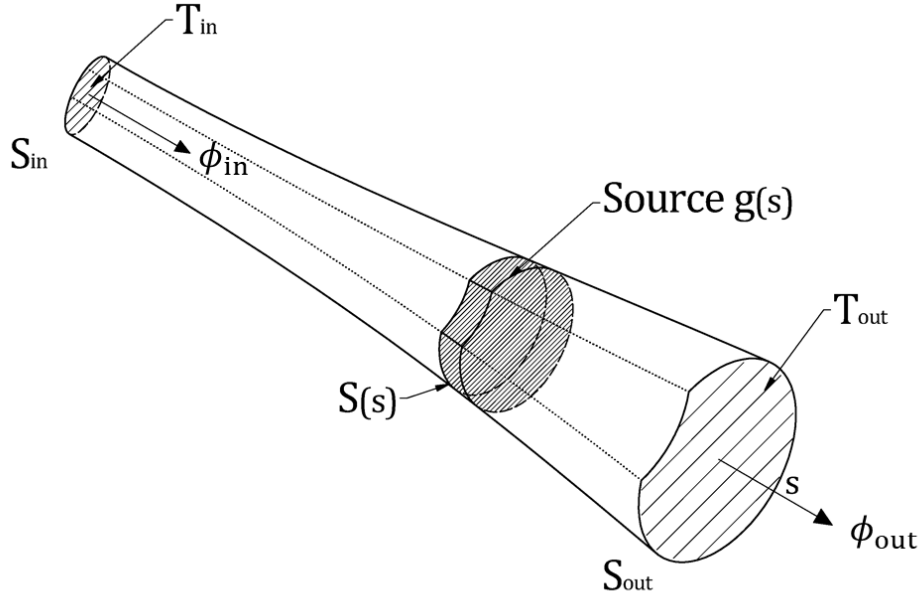


Figure 7: Unidirectional conduction with internal sources

98

99 Integrating equation (5) from  $s_{in}$  to  $s_{out}$ , we get:

$$\phi_{out} = Q + \phi_{in} \quad (6)$$

100 Integrating equation (4) from  $s_{in}$  to  $s_{out}$  yields:

$$T_{in} - T_{out} = R\phi_{out} - \int_{s_{in}}^{s_{out}} r(s)g(s)S(s)ds \quad (7)$$

101 As demonstrated in [37], relations (6) and (7) correspond to the thermal circuit shown in figure 8,  
 102 which shows that a medium with an internal heat source can be represented using an equivalent  
 103 thermal circuit with two resistances  $\beta R$  and  $(1 - \beta)R$ , where the total rate of heat generation  $Q$  is  
 104 dissipated between the two resistances. Therefore:

$$\beta = \int_{s_{in}}^{s_{out}} \frac{r(s)}{R} \frac{g(s)}{Q} S(s)ds \quad (8)$$

105  $\beta$  is the partition coefficient and  $Q$  is the total rate of heat generation in the medium.

106 In this representation,  $\beta$  is independent of the medium's thermal conductivity and is only a function  
 107 of the source's distribution.

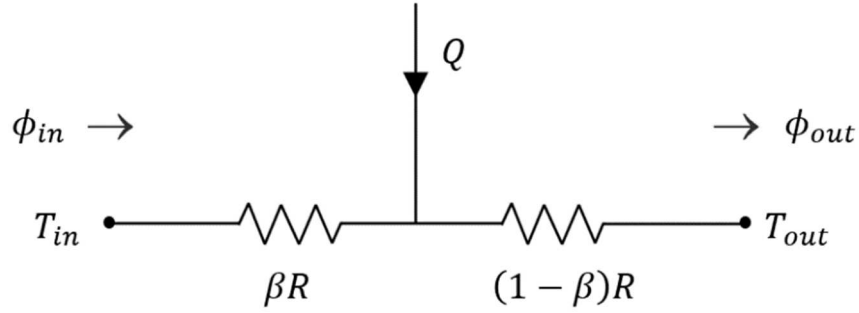


Figure 8: Equivalent thermal circuit of heat conduction in a medium with an internal heat source

108

109 **4. Application to electrothermal problems:**

110 With reference to figure 7, we consider the problem of heat generation due to Joule heating which  
 111 represents the conversion from electrical to thermal energy in a current-carrying medium. An electric  
 112 potential difference is imposed between  $S_{in}$  and  $S_{out}$ , thus an electric current  $I$  flows through the  
 113 medium. Considering  $\rho_e$  the electrical resistivity of the medium, the electrical resistance of an element  
 114  $ds$  is expressed in the same way as the thermal resistance (solution of the same problem,  $\Delta T = 0$  or  
 115  $\Delta V = 0$ , for the same volume and boundary conditions):

116 
$$dr_e = \frac{\rho_e ds}{S(s)}$$

117 Thus

$$g(s) = \frac{\rho_e ds}{S(s)} I^2 \frac{1}{S(s) ds} = \frac{\rho_e I^2}{S^2(s)} \quad (9)$$

118 Relation (8) becomes:

$$\beta = \frac{\int_{S_{in}}^{S_{out}} \frac{ds}{\lambda S(s)} \frac{\rho_e I^2}{S^2(s)}}{\int_{S_{in}}^{S_{out}} \frac{ds}{\lambda S(s)} \int_{S_{in}}^{S_{out}} \frac{\rho_e I^2}{S^2(s)} S(s) ds} \quad (10)$$

119 Which reduces to

$$\beta = \frac{\int_{S_{in}}^{S_{out}} \frac{ds}{S(s)} \cdot \frac{ds}{S(s)}}{\left( \int_{S_{in}}^{S_{out}} \frac{ds}{S(s)} \right)^2} \quad (11)$$

120 Let  $F(s) = \int_{S_{in}}^s \frac{ds}{S(s)}$  (with  $F(S_{in}) = 0$ ), we get:

$$\beta = \frac{1}{F^2(S_{out})} \int_{S_{in}}^{S_{out}} F(s) F'(s) ds = \frac{1}{2} \quad (12)$$

121 The partition coefficient  $\beta$  is a constant equal to  $1/2$ . This remarkable result can be demonstrated for  
 122 the general electrothermal problem (steady or transient) with any geometrical configuration (see [37]).

123 **5. Thermal contact with heat sources:**



124 Let's consider the circuit shown in figure 5. In the presence of heat sources in the internal and external  
 125 branches, the potentials  $A$  and  $C$  are no longer identical and the same is true for potentials  $B$  and  $D$ .  
 126 This prevents, in the general case, the definition of the contact resistance.

127 Let's consider the two following particular cases.

128 **5.1. Fluid with a high thermal resistance:**

129 An example is the thermal contact in a vacuum environment. For this case, the circuit in figure 5  
 130 reduces to one branch (internal) with heat sources and we can use the preceding result shown in figure  
 131 8. The thermal equivalent circuit for this case is shown in figure 10 where:

132 
$$R_1 = R_{m1} + R_{c1} + R_{a1}$$

133 And

134 
$$R_2 = R_{m2} + R_{c2} + R_{a2}$$

135  $R_1$  and  $R_2$  are respectively the total thermal resistances of medium 1 and 2.  $T_c$  is the contact  
 136 temperature. Note that in the circuit of figure 10, the only approximation is that the contact is  
 137 isothermal.

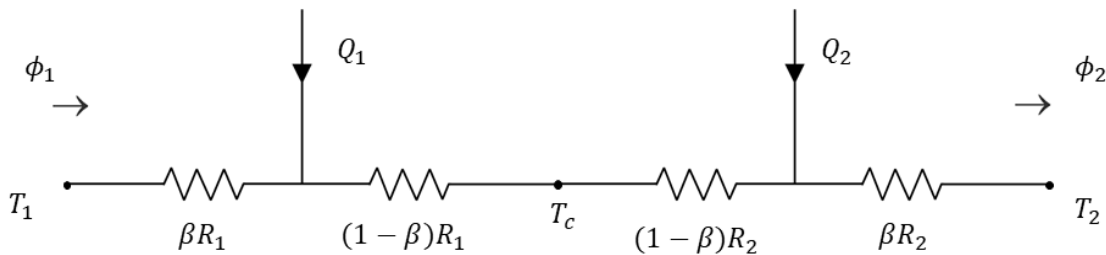


Figure 10: Equivalent thermal circuit of thermal contact with heat source and  $R_f \rightarrow \infty$

138 **5.2. Fluid with a non-negligible thermal resistance:**

139 In this case, the solution is obtained by exploiting the linearity of the problem. The temperature is then  
 140 written in the form  $T = X + Y$ . For the problem in  $X$ , there is a temperature difference ( $T_1 \neq T_2$ ) with  
 141 no heat source, while for the problem in  $Y$ , there is a heat source without temperature difference  
 142 ( $T_1 = T_2$ ). The solution to the problem in  $X$  is given by figure 6. The solution to the problem in  $Y$  can  
 143 be simplified if we assume that the heat transfer through the external region is negligible (this  
 144 hypothesis will be later verified using numerical simulations), thus, the solution to the problem in  $Y$  is  
 145 given by figure 10 where  $T_1 = T_2 = 0$ . The equivalent thermal circuits for this case are shown in figure  
 146 11.

147 The heat transfer rates are:

$$\phi_1 = \phi_X + \phi_{Y1} \tag{13}$$

$$\phi_2 = \phi_X + \phi_{Y2} \tag{14}$$

148 And the contact temperature

$$T_c = X_c + Y_c \tag{15}$$

149 For electrothermal problems, we only need to use  $\beta = 1/2$ .

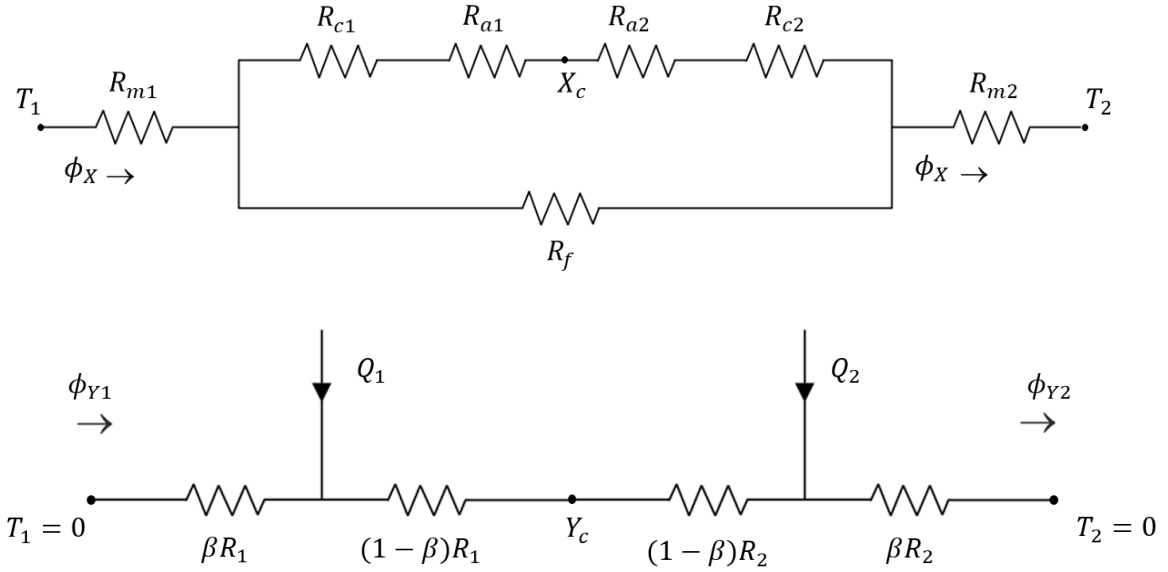


Figure 11: Equivalent thermal circuit for thermal contacts with heat source and interstitial fluid

150

151 **6. Numerical simulations and comparison to the macroscopic approach: application to an**  
 152 **elementary contact cell**

153 In this section, the results of the analytical approach are compared to numerical simulations for the  
 154 elementary contact cell described in figure 12. The height  $l_1$  and  $l_2$  are sufficiently larger than the  
 155 radius  $a$  so that the constriction is fully developed; the radius  $b$  is sufficiently small as to obtain a  
 156 realistic model.

157 The geometrical parameters are:

158 
$$a = 10 \mu m ; b = 1 \mu m ; l_1 = l_2 = 20 \mu m$$

159 Two materials are considered, Iron and Copper, the interstitial fluid is air. The relevant physical  
 160 properties are listed below:

- 161 • Iron:  $\lambda = 40 Wm^{-1} K^{-1}$  and  $\rho_e = 10^{-7} \Omega m$   
 162 • Copper:  $\lambda = 400 Wm^{-1} K^{-1}$  and  $\rho_e = 2 \cdot 10^{-8} \Omega m$   
 163 • Air:  $\lambda_f = 0.025 Wm^{-1} K^{-1}$  and  $\rho_e = 1.24 \cdot 10^{14} \Omega m$

164 We define three interface configurations:

- 165 • Configuration 1: Asperities with nil thickness  $\delta_1 = \delta_2 = 0$  without any interstitial fluid  
 166 • Configuration 2: Asperities of thickness  $\delta_1 = \delta_2 = 0.5 \mu m$  without interstitial fluid  
 167 • Configuration 3: Asperities of thickness  $\delta_1 = \delta_2 = 0.5 \mu m$  with air as interstitial fluid

168 And four different cases:

- 169 • Case 1: iron to iron contact with  $T_1 = T_2 = 0^\circ C$  and  $\Delta U = 4.24 \cdot 10^{-2} V$   
 170 • Case 2: iron to copper contact with  $T_1 = T_2 = 0^\circ C$  and  $\Delta U = 4.24 \cdot 10^{-2} V$   
 171 • Case 3: iron to iron contact with  $T_1 = 100^\circ C$ ,  $T_2 = 0^\circ C$  and  $\Delta U = 4.24 \cdot 10^{-2} V$   
 172 • Case 4: iron to copper contact with  $T_1 = 100^\circ C$ ,  $T_2 = 0^\circ C$  and  $\Delta U = 4.24 \cdot 10^{-2} V$

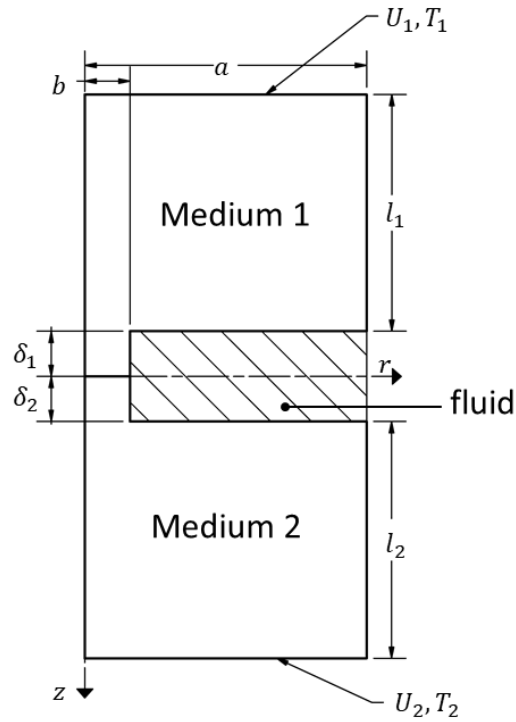


Figure 12: Thermal contact with heat source in an axisymmetric elementary cell

173

### 6.1. Numerical results:

174

The numerical simulations are carried out using FLUENT, the geometry is modeled exploiting its axisymmetry. The computational domains are meshed with triangle and quadrilateral elements. the conformal mesh is locally refined at the interface. For each case, a mesh sensitivity test was conducted where the optimal mesh is adopted. The energy and electric potential equations are iteratively solved. The convergence was judged by monitoring residuals and key quantities such as the temperature and potential at the interface ( $T_c$  and  $U_c$ ). The numerical results are summarized in table 1.

179

180

Table 1: Numerical results				
Configuration 1: Asperities with nil thickness $\delta_1 = \delta_2 = 0$				
Parameter	Case 1	Case 2	Case 3	Case 4
	Iron	Iron	Iron	Iron
	Iron	Copper	Iron	Copper
$\Delta U (V)$	0.0424	0.0424	0.0424	0.0424
$\Delta T$	0	0	100	100
$\phi_1(W)$	-0.01595	-0.02475	-0.00893	-0.01175
$\phi_2(W)$	0.01596	0.02884	0.02323	0.04185
$U_c(V)$	0.0212	0.0072	0.0212	0.0072
$T_c(^{\circ}C)$	55.41	17.04	106.25	26.14
$I (A)$	0.76	1.26	0.76	1.26
Configuration 2: Asperities of thickness $\delta_1 = \delta_2 = 0.5 \mu m$ without interstitial fluid				
Parameter	Case 1	Case 2	Case 3	Case 4
	Iron	Iron	Iron	Iron
	Iron	Copper	Iron	Copper
$\Delta U (V)$	0.0424	0.0424	0.0424	0.0424
$\Delta T$	0	0	100	100
$\phi_1(W)$	-0.01000	-0.01541	-0.00555	-0.00732
$\phi_2(W)$	0.01000	0.01793	0.01445	0.02603
$U_c(V)$	0.0212	0.0071	0.0212	0.0071
$T_c(^{\circ}C)$	56.17	17.03	106.19	26.12
$I (A)$	0.47	0.79	0.47	0.79
Configuration 3: Asperities of thickness $\delta_1 = \delta_2 = 0.5 \mu m$ with air as interstitial fluid				
Parameter	Case 1	Case 2	Case 3	Case 4
	Iron	Iron	Iron	Iron
	Iron	Copper	Iron	Copper
$\Delta U (V)$	0.0424	0.0424	0.0424	0.0424
$\Delta T$	0	0	100	100
$\phi_1(W)$	-0.00993	-0.01519	-0.00495	-0.00659
$\phi_2(W)$	0.00993	0.01800	0.01491	0.02659
$U_c(V)$	0.0212	0.0072	0.0212	0.0072
$T_c(^{\circ}C)$	56.31	17.69	106.31	27.15
$I (A)$	0.47	0.78	0.47	0.78

181

182

## 6.2. Calculation of thermal resistances:

183

184

185

186

$R_{m1}$ ,  $R_{m2}$ ,  $R_{a1}$ ,  $R_{a2}$  and  $R_f$  are wall type resistances, that is, they take the form  $e/\lambda S$  where  $e$  is the wall thickness,  $\lambda$  its conductivity and  $S$  the heat transfer area.  $R_{c1}$  and  $R_{c2}$  are the constrictions resistances and depend on the boundary condition at the contact interface. The classical approach [38] shows that there are two limiting conditions that correspond to 'uniform heat flux' and 'uniform

187 temperature'. The analytical solutions obtained in the form of series were approximated and  
 188 presented in a practical manner by various authors, here we will use the following formulas proposed  
 189 in [38]:

Uniform temperature 
$$R_c = \frac{1}{4\lambda r} f\left(\frac{r}{R}\right) \quad (16)$$

Uniform heat flux 
$$R_c = \frac{8}{3\pi^2\lambda r} f\left(\frac{r}{R}\right) \quad (17)$$

190 With

191 
$$f\left(\frac{r}{R}\right) = 1 - 1.288\frac{r}{R} + 0.288\left(\frac{r}{R}\right)^{3.75}$$

192 In the following we will show that the deviation between the analytical and numerical results comes  
 193 solely from the approximate calculation of the constriction resistances. We will also use the resistances  
 194 obtained using numerical simulations.

195 **6.3. Configuration 1: Asperities with nil thickness  $\delta_1 = \delta_2 = 0$ :**

196 **6.3.1. Thermal resistances**

197 The thermal resistances values for Iron are presented below, in  $K/W$ . For copper, the resistances can  
 198 be obtained by dividing the values below by 10 ( $\lambda_{copper}/\lambda_{iron} = 10$ ).

$R_m$	$R_a$	$R_c$ (Analytical calculations for a uniform heat flux)	$R_c$ (Analytical calculations for a uniform temperature)	$R_c$ (Numerical simulations)
1591.5	0	5885	5445	5400

199 **6.3.2. Analytical-numerical comparison**

200 In this configuration, the interface temperature is uniform as demonstrated in [35] and confirmed by  
 201 the numerical results as shown in figure 13. The numerical temperature at  $z = \delta_1$  is plotted against  
 202 the radius ( $0 \leq r \leq b$ ). The small deviations are caused by the singularity at  $r = b$ .

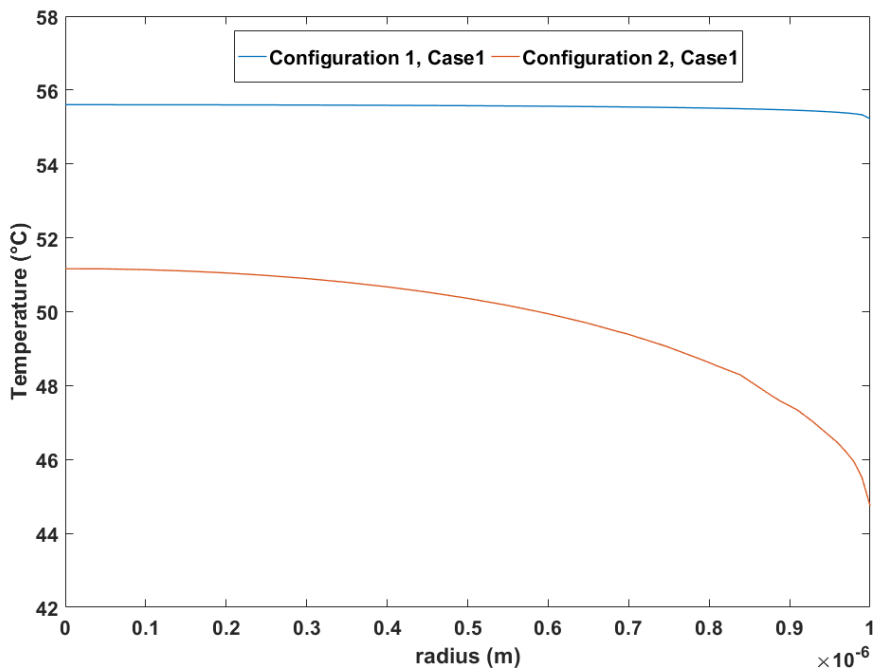


Figure 13: Temperature profile at  $z = \delta_1$  for configuration 1, case 1 and configuration 2, case 1.

203 The overall results for this configuration are summarized in table 2. The ‘analytical-numerical’ method  
 204 is about using the analytical approach with the numerically obtained thermal resistances. The  
 205 ‘analytical-analytical’ method uses the analytical approach with the constriction resistance evaluated  
 206 through equations (16) and (17), the first and second lines contain respectively the results for a  
 207 ‘uniform temperature’ and a ‘uniform heat flux’ interfacial boundary conditions. The detailed  
 208 calculations are presented in appendix 2.

Method	Parameter	Case 1	Case 2	Case 3	Case 4	
		Iron-Iron	Iron-Copper	Iron-Iron	Iron-Copper	
Numerical	$\phi_1(mW)$	-15.95	-24.75	-8.93	-11.75	
	$\phi_2(mW)$	15.96	28.84	23.23	41.85	
	$T_c(^{\circ}C)$	55.40	17.04	106,2	26.14	
Numerical- Analytical	$\phi_1(mW)$	-16.06	-24.74	-8.91	-11.74	
	$\phi_2(mW)$	16.06	28.81	23.21	41.80	
	$T_c(^{\circ}C)$	56.1	17.02	106.1	26.11	
Analytical- Analytical	$\phi_1(mW)$	Eq (16)	-16.06	-24.73	-8.95	-11.82
		Eq (17)	-16.06	-24.74	-9.37	-12.58
	$\phi_2(mW)$	Eq (16)	16.06	28.81	23.77	41.72
		Eq (17)	16.06	28.81	22.75	40.96
	$T_c(^{\circ}C)$	Eq (16)	56.5	17.13	106.5	26.22
		Eq (17)	60.0	18.20	110.9	27.29

209

210 From the foregoing, it is clear that there is a good agreement between the numerical and analytical  
 211 ‘uniform temperature’ approach, for both the heat transfer rates and interface temperatures.

#### 212 **6.4. Configuration 2: Asperities of thickness $\delta_1 = \delta_2 = 0.5 \mu m$ without interstitial fluid:**

##### 213 **6.4.1. Thermal resistances**

214 The thermal resistances values for Iron are reported below, in  $K/W$ . For copper, the resistances can  
 215 be obtained by dividing the values below by 10 ( $\lambda_{copper}/\lambda_{iron} = 10$ ).

$R_m$	$R_a$	$R_c$ (Analytical calculations for a uniform heat flux)	$R_c$ (Analytical calculations for a uniform temperature)	$R_c$ (Numerical simulations)
1591.5	3978.8	5885	5445	5664.31

##### 216 **6.4.2. Analytical-numerical comparison**

217 In this configuration, the temperature at  $z = \delta_1$  is not uniform (see figure 13). This is also confirmed  
 218 from the preceding values for the contact resistances where the numerical contact resistance is  
 219 between the two analytical contact resistances.

220 The results are presented in table 3, there is a perfect analytical-numerical agreement by using the  
 221 numerical constriction resistances in the analytical calculations. When using the analytical constriction  
 222 resistances in the analytical calculations, the maximum relative deviation is less than 2%.

Table 3: Numerical and analytical comparison for configuration 2: Asperities of thickness  $\delta_1 = \delta_2 = 0.5 \mu m$  without interstitial fluid

Method	Parameter	Case 1	Case 2	Case 3	Case 4	
		Iron-Iron	Iron-Copper	Iron-Iron	Iron-Copper	
Numerical	$\phi_1(mW)$	-10.00	-15.41	-5.55	-7.32	
	$\phi_2(mW)$	10.00	17.93	14.45	26.03	
	$T_c(^{\circ}C)$	56.17	17.03	106.2	26.12	
Numerical-Analytical	$\phi_1(mW)$	-10.00	-15.40	-5.55	-7.31	
	$\phi_2(mW)$	10.00	17.93	14.45	26.02	
	$T_c(^{\circ}C)$	56.16	17.02	106.1	26.11	
Analytical-Analytical	$\phi_1(mW)$	Eq (16)	-10.00	-15.40	-5.46	-7.15
		Eq (17)	-10.00	-15.40	-5.63	-7.46
	$\phi_2(mW)$	Eq (16)	10.00	17.93	14.54	26.18
		Eq (17)	10.00	17.93	14.36	25.86
	$T_c(^{\circ}C)$	Eq (16)	55.07	16.69	105.0	25.78
		Eq (17)	57.27	17.35	107.3	26.44

223

### 6.5. Configuration 3: Asperities of thickness $\delta_1 = \delta_2 = 0.5 \mu m$ with air as interstitial fluid

224

#### 6.5.1. Thermal resistances

225

226 The thermal resistances values for Iron are reported below, in  $K/W$ . For copper, the resistances can  
 227 be obtained by dividing the values below by 10 ( $\lambda_{copper}/\lambda_{iron} = 10$ ).

$R_m$	$R_a$	$R_f$	$R_c$ (Analytical calculations for a uniform heat flux)	$R_c$ (Analytical calculations for a uniform temperature)	$R_c$ Numerical simulations
1591.5	3978.8	128610	5885	5445	5664.31

228

#### 6.5.2. Analytical-numerical comparison

229

230 Here, the analytical calculations are done using the superposition principle as shown in section 4.2 and  
 231 represented in figure 11 with  $\beta = 1/2$ .

232 The results for this configuration are reported in table 4. There is a good analytical-numerical  
 233 agreement. Taking the numerical results as a reference, the numerical-analytical and analytical-  
 234 analytical methods have maximum deviations of less than 1% and 4% respectively.

Table 4: Numerical and analytical comparison for configuration 2: Asperities of thickness  $\delta_1 = \delta_2 = 0.5 \mu m$  with air as interstitial fluid

Method	Parameter	Case 1	Case 2	Case 3	Case 4	
		Iron-Iron	Iron-Copper	Iron-Iron	Iron-Copper	
Numerical	$\phi_1(mW)$	-9.93	-15.19	-4.95	-6.59	
	$\phi_2(mW)$	9.93	18.00	14.91	26.59	
	$T_c(^{\circ}C)$	56.31	17.69	106.3	27.15	
Numerical-Analytical	$\phi_1(mW)$	-9.91	-15.26	-4.90	-6.60	
	$\phi_2(mW)$	9.91	17.76	14.92	26.42	
	$T_c(^{\circ}C)$	55.66	16.87	105.70	25.96	
Analytical-Analytical	$\phi_1(mW)$	Eq (16)	-9.91	-15.26	-4.81	-6.45
		Eq (17)	-9.91	-15.26	-4.98	-6.76
	$\phi_2(mW)$	Eq (16)	9.91	17.76	15.00	26.58
		Eq (17)	9.91	17.76	14.84	26.27
	$T_c(^{\circ}C)$	Eq (16)	54.57	16.54	104.6	25.63
		Eq (17)	56.75	17.20	106.7	26.29

235

## 236 7. Conclusion:

237 In this work, it was shown that it is possible to use the ‘contact resistance’ concept to describe solid-  
 238 solid contact with heat sources. This is done by using the notion of heat transfer partition coefficient.  
 239 For electrothermal problems, we demonstrated that the partition coefficient is a constant equal to  $\frac{1}{2}$   
 240 whatever the system’s geometrical configuration.

241 Numerical simulations were carried out for various thermal contact configurations with different cases.  
 242 The excellent agreement between the numerical and analytical results demonstrates the validity of  
 243 the proposed approach, which also allows to obtain the interface temperature using a simple thermal-  
 244 electrical analogy. The deviation between Numerical and analytical results comes mainly from the  
 245 calculation of the constriction resistances.

## 246 Nomenclature

247 *Latin symbols*

$T$	Temperature, K
$Q$	Rate of heat generation, W
$S$	Surface, $m^2$
$R$	Thermal resistance, K/W
$V$	Volume, $m^3$
$s$	Curvilinear coordinate, m
$g$	Volumetric heat generation rate, $W/m^3$
$e$	Wall thickness, m
$U$	Electrical potential, V

248 *Greek symbols*

$\phi$	Heat transfer rate, W
$\lambda$	Thermal conductivity, $W/(m K)$
$\rho_e$	Electrical resistivity, $\Omega m$
$\beta$	Partition coefficient
$\alpha$	heat generation factor
$\phi_g$	the total rate of heat generation (W)



<i>in</i>	inlet
<i>out</i>	outlet
<i>i</i>	internal
<i>e</i>	external
<i>m</i>	medium
<i>a</i>	asperity
<i>f</i>	fluid

250

251 **Appendix 1:**

252 To demonstrate that  $A = C$  and  $B = D$  (see figure 5), we only need to consider the hypothesis of a  
 253 fully developed constriction, i.e. the heat flux in  $l_2$  and  $l_1$  is uniform ( $l_1$  and  $l_2$  are sufficiently larger  
 254 than  $b$ ). With reference to figure 5, we can write:

255 
$$T_1 - A = R_{m1i}\phi_i = R_{m1i}\phi_i S_i = \frac{l_1}{\lambda_1 S_i} \phi_i S_i = \frac{l_1}{\lambda_1} \phi_i$$

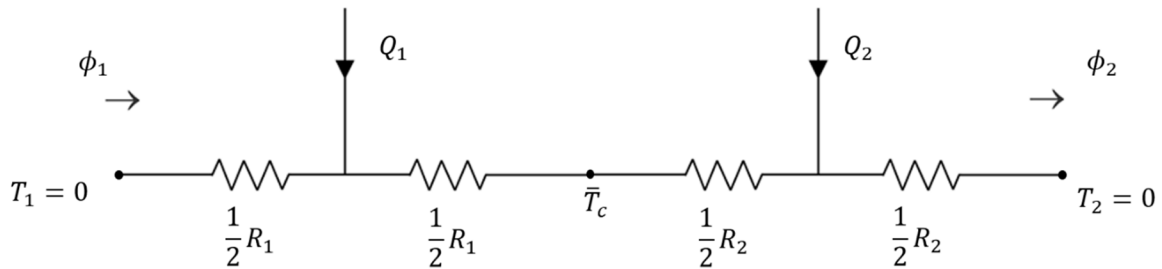
256 
$$T_1 - C = R_{m1e}\phi_e = R_{m1e}\phi_e S_e = \frac{l_1}{\lambda_1 S_e} \phi_e S_e = \frac{l_1}{\lambda_1} \phi_e$$

257 Or  $\phi_i = \phi_e$  (uniform heat flux)

258 Therefore  $A = C$ . In a similar manner, we can demonstrate that  $B = D$ .

259 **Appendix 2:**

260 **I. Calculations of the heat transfer rates and the interface temperature ( $T_1 = T_2 = 0$  with**  
 261 **heat source)**



262

263 
$$\phi_1 = -Q_1 \frac{R_1 + 2R_2}{2(R_1 + R_2)} - Q_2 \frac{R_2}{2(R_1 + R_2)}$$

264 
$$\phi_2 = Q_1 \frac{R_1}{2(R_1 + R_2)} + Q_2 \frac{2R_1 + R_2}{2(R_1 + R_2)}$$

265 
$$Q_1 = \frac{R_1^e}{R_1^e + R_2^e} Q \quad \text{and} \quad Q_2 = \frac{R_2^e}{R_1^e + R_2^e} Q$$

266 The superscript  $e$  stands for electrical resistance. Knowing that

267 
$$R_1^e = \rho_1 \lambda_1 R_1$$

268 And

269  $R_2^e = \rho_2 \lambda_2 R_2$

270 Substituting and rearranging we obtain the heat transfer rates:

271 
$$\phi_1 = -\frac{Q}{2} \left[ \frac{\rho_1 \lambda_1 R_1^2 + \rho_2 \lambda_2 R_2^2 + 2\rho_1 \lambda_1 R_1 R_2}{(R_1 + R_2)(\rho_1 \lambda_1 R_1 + \rho_2 \lambda_2 R_2)} \right]$$

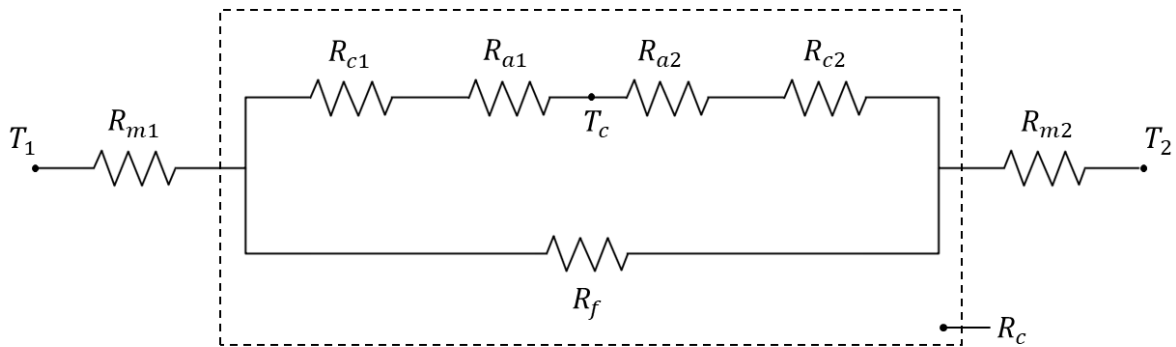
272 
$$\phi_1 = \frac{Q}{2} \left[ \frac{\rho_1 \lambda_1 R_1^2 + \rho_2 \lambda_2 R_2^2 + 2\rho_2 \lambda_2 R_1 R_2}{(R_1 + R_2)(\rho_1 \lambda_1 R_1 + \rho_2 \lambda_2 R_2)} \right]$$

273 And the interface temperature

274 
$$T_c = \frac{R_1 R_2 (Q_1 + Q_2)}{2(R_1 + R_2)} = \frac{Q}{2 \left( \frac{1}{R_1} + \frac{1}{R_2} \right)}$$

275 In the last expression, we can see that the interface temperature depends only on the rate of heat  
276 generation

277 **II. Calculations of the heat transfer rates and the interface temperature ( $T_1 \neq T_2$  without heat  
278 source)**



279

280 
$$\phi = \frac{T_1 - T_2}{R_T} = \frac{\Delta T}{R_T}$$

281 With

282 
$$R_T = R_{m1} + R_{m2} + \frac{(R_{c1} + R_{a1} + R_{c2} + R_{a2})R_f}{R_{c1} + R_{a1} + R_{c2} + R_{a2} + R_f}$$

283 We can also write

284 
$$T_c = \frac{\Delta T}{R_T} \left[ R_{m2} + \frac{(R_{c2} + R_{a2})R_f}{R_{c1} + R_{a1} + R_{c2} + R_{a2} + R_f} \right]$$

285 In the case where medium 1 and medium 2 have identical geometrical parameters:

286 
$$R_{m1} = \frac{K}{\lambda_1} \quad , \quad R_{m2} = \frac{K}{\lambda_2}$$

287 
$$R_{c1} + R_{a1} = \frac{K'}{\lambda_1} \quad , \quad R_{c2} + R_{a2} = \frac{K'}{\lambda_2}$$

288 Let's consider  $R_u = R_{c1} + R_{a1} + R_{c2} + R_{a2} + R_f$

289 Therefore

$$290 \quad R_T = (R_{m1} + R_{m2}) \left[ 1 + \frac{\frac{R_{c1} + R_{a1} + R_{c2} + R_{a2}}{R_{m1} + R_{m2}} R_f}{R_u} \right]$$

291 And

$$292 \quad T_c = \Delta T \frac{R_{m2}}{R_{m1} + R_{m2}} \left[ \frac{1 + \frac{\frac{R_{c2} + R_{a2}}{R_{m2}} R_f}{R_u}}{\frac{R_{c1} + R_{a1} + R_{c2} + R_{a2}}{R_{m1} + R_{m2}} R_f} \right]$$

293 With

$$294 \quad \frac{R_{c2} + R_{a2}}{R_{m2}} = \frac{K'}{\lambda_2} \cdot \frac{\lambda_2}{K} = \frac{K'}{K}$$

295 And

$$296 \quad \frac{R_{c1} + R_{a1} + R_{c2} + R_{a2}}{R_{m1} + R_{m2}} = \frac{\frac{K'}{\lambda_1} + \frac{K'}{\lambda_2}}{\frac{K}{\lambda_1} + \frac{K}{\lambda_2}} = \frac{K'}{K}$$

297 Thus

$$298 \quad T_c = \Delta T \frac{R_{m2}}{R_{m1} + R_{m2}} \left[ \frac{1 + \frac{K' R_f}{K R_u}}{1 + \frac{K' R_f}{K R_u}} \right]$$

$$299 \quad T_c = \Delta T \frac{R_{m2}}{R_{m1} + R_{m2}}$$

300 In the last expression, we can see that the interface temperature does not depend on  $R_f$  (fluid  
301 resistance).

## 302 References

- 303 1. Kato, T., & Fujii, H. (1999). Energy partition in conventional surface grinding. *Journal of*  
304 *Manufacturing Science and Engineering*, 121(3), 393-398.
- 305 2. Chandraseker, S., Farris, T. N., Hebbbar, R. R., & Hucker, S. (1994). Thermal aspects of surface  
306 finishing processes. *ASM International, Member/Customer Service Center, Materials Park, OH*  
307 *44073-0002, USA, 1994.*, 152-157.
- 308 3. Grzesik, W. (1998). The role of coatings in controlling the cutting process when turning with coated  
309 indexable inserts. *Journal of Materials Processing Technology*, 79(1-3), 133-143.
- 310 4. Grzesik, W., & Nieslony, P. (2003). A computational approach to evaluate temperature and heat  
311 partition in machining with multilayer coated tools. *International Journal of Machine Tools and*  
312 *Manufacture*, 43(13), 1311-1317.
- 313 5. Kulchitsky-Zhyhailo, R., & Yevtushenko, A. (1998). Axi-symmetric contact problem with frictional  
314 heating for thermally nonlinear sliders. *International journal of mechanical sciences*, 40(11), 1133-  
315 1143.

- 316 6. Kulchytsky-Zhyhailo, R. (2001). A simplified solution for three-dimensional contact problem with  
317 heat generation. *International journal of engineering science*, 39(3), 303-315.
- 318 7. Pauk, V., & Yevtushenko, A. (1997). Periodical contact problems for a half-space involving frictional  
319 heating. *International journal of mechanical sciences*, 39(1), 87-95.
- 320 8. Pauk, V. J. (1999). Plane contact problem for a layer involving frictional heating. *International*  
321 *journal of heat and mass transfer*, 42(14), 2583-2589.
- 322 9. Grylitsky, D. V., & Pauk, V. J. (1995). Some quasistationary contact problems for half-space  
323 involving heat generation and radiation. *International journal of engineering science*, 33(12), 1773-  
324 1781.
- 325 10. Yevtushenko, A. A., & Kulchytsky-Zhyhailo, R. D. (1995). Axi-symmetrical transient contact problem  
326 for sliding bodies with heat generation. *International journal of solids and structures*, 32(16), 2369-  
327 2376.
- 328 11. Mazo, L., Cassagne, B., Badie-Levet, D., & Bardon, J. P. (1978). Etude des conditions de liaison  
329 thermique dans le cas du frottement sec métal-plastique. *Rev. Gén. Therm*, 204, 919-933.
- 330 12. Kulchytsky-Zhyhailo, R. D., & Yevtushenko, A. A. (1997). Thermoelastic contact problems with  
331 frictional heating and convective cooling. *International journal of engineering science*, 35(3), 211-  
332 219.
- 333 13. Komanduri, R., & Hou, Z. B. (2001). Analysis of heat partition and temperature distribution in  
334 sliding systems. *Wear*, 251(1-12), 925-938.
- 335 14. Komanduri, R., & Hou, Z. B. (2001). Thermal analysis of dry sleeve bearings—a comparison  
336 between analytical, numerical (finite element) and experimental results. *Tribology*  
337 *International*, 34(3), 145-160.
- 338 15. Barber, J. R. (1967). Distribution of heat between sliding surfaces. *Journal of Mechanical*  
339 *Engineering Science*, 9(5), 351-354.
- 340 16. Kounas, P. S., Dimarogonas, A. D., & Sandor, G. N. (1972). The distribution of friction heat between  
341 a stationary pin and a rotating cylinder. *Wear*, 19(4), 415-424.
- 342 17. Levytskyi, V. P., & Onyshkevych, V. M. (1996). Plane contact problem with heat generation account  
343 of friction. *International journal of engineering science*, 34(1), 101-112.
- 344 18. Ciavarella, M., Johansson, L., Afferrante, L., Klarbring, A., & Barber, J. R. (2003). Interaction of  
345 thermal contact resistance and frictional heating in thermoelastic instability. *International Journal*  
346 *of Solids and Structures*, 40(21), 5583-5597.
- 347 19. Bardon, J. P. (1994). Bases physiques des conditions de contact thermique imparfait entre milieux  
348 en glissement relatif. *Revue générale de thermique*, 33(386).
- 349 20. Chantrenne, P., & Raynaud, M. (1997). A microscopic thermal model for dry sliding  
350 contact. *International journal of heat and mass transfer*, 40(5), 1083-1094.
- 351 21. Bauzin, J. G., & Laraqi, N. (2004). Simultaneous estimation of frictional heat flux and two thermal  
352 contact parameters for sliding contacts. *Numerical Heat Transfer, Part A: Applications*, 45(4), 313-  
353 328.
- 354 22. Laraqi, N. (1992). Contact temperature and flux partition-coefficient of heat generated by dry friction  
355 between 2 solids—new approach to flux generation. *International Journal of Heat and Mass*  
356 *Transfer*, 35(11), 3131-3139.
- 357 23. Guillot, E., Bourouga, B., Garnier, B., & Dubar, L. (2007, April). Experimental study of thermal sliding  
358 contact with friction: application to high speed machining of metallic materials. In *AIP Conference*  
359 *Proceedings* (Vol. 907, No. 1, pp. 1263-1268). AIP.
- 360 24. Chantrenne, P., & Raynaud, M. (2001). Study of a macroscopic sliding contact thermal model from  
361 microscopic models. *International journal of thermal sciences*, 40(7), 603-621.
- 362 25. Han, Z., Orozco, J., Indacochea, J. E., & Chen, C. H. (1989). Resistance spot welding: a heat transfer  
363 study. *Welding journal*, 68(9), 363s-371s.

- 364 26. Cho, H. S., & Cho, Y. J. (1989). A study of the thermal behavior in resistance spot welds. *Welding*  
365 *Journal*, 68(6), 236s-244s.
- 366 27. Khan, J. A., Xu, L., Chao, Y. J., & Broach, K. (2000). Numerical simulation of resistance spot welding  
367 process. *Numerical Heat Transfer: Part A: Applications*, 37(5), 425-446.
- 368 28. Wang, S. C., & Wei, P. S. (2001). Modeling dynamic electrical resistance during resistance spot  
369 welding. *Journal of heat transfer*, 123(3), 576-585.
- 370 29. Le Meur, G., Bourouga, B., & Dupuy, T. (2003). Measurement of contact parameters at  
371 electrode/sheet interface during resistance spot welding process. *Science and technology of*  
372 *welding and joining*, 8(6), 415-422.
- 373 30. Le Meur, G., Bourouga, B., & Bardon, J. P. (2006). Microscopic analysis of interfacial electrothermal  
374 phenomena—definition of a heat generation factor. *International journal of heat and mass*  
375 *transfer*, 49(1-2), 387-401.
- 376 31. Feulvarch, E., Robin, V., & Bergheau, J. M. (2004). Resistance spot welding simulation: a general  
377 finite element formulation of electrothermal contact conditions. *Journal of Materials Processing*  
378 *Technology*, 153, 436-441.
- 379 32. Rogeon, P., Carre, P., Costa, J., Sibilia, G., & Saindrenan, G. (2008). Characterization of electrical  
380 contact conditions in spot welding assemblies. *Journal of Materials Processing Technology*, 195(1-  
381 3), 117-124.
- 382 33. Rogeon, P., Raelison, R., Carre, P., & Dechalotte, F. (2009). A microscopic approach to determine  
383 electrothermal contact conditions during resistance spot welding process. *Journal of Heat*  
384 *Transfer*, 131(2), 022101.
- 385 34. Degiovanni, A. G. M. L. A., Sinicki, G., Gery, A., & Laurent, M. (1984). Un modèle de résistance  
386 thermique de contact en régime permanent. *Revue générale de thermique*, 23(267), 161-175.
- 387 35. Degiovanni, A., & Moyne, C. (1989). Résistance thermique de contact en régime permanent:  
388 influence de la géométrie de contact. *Revue générale de thermique*, 28(334), 557-564.
- 389 36. Degiovanni, A., Remy, B., & Andre, S. (2003). Thermal resistance of a multi-constrictions contact:  
390 A simple model. *International journal of heat and mass transfer*, 46(19), 3727-3735.
- 391 37. El Maakoul, A., Moyne, C., & Degiovanni, A. (2019). A general approach to solve heat conduction  
392 problems with internal heat sources using resistance and quadrupole concepts. *International*  
393 *Journal of Heat and Mass Transfer*, 129, 793-800.
- 394 38. Maillet, D. (2000). Thermal quadrupoles: solving the heat equation through integral transforms.  
395 John Wiley & Sons Inc.